IJAME
Int. J. of Applied Mechanics and Engineering, 2026, vol.31, No.4, pp.109-128
DOI: 10.59441/ijame/221498

UNSTEADY CARREAU FLUID FLOW IN THREE-DIMENSIONAL MAGNETOHYDRODYNAMICS WITH A VISCOUS DISSIPATION EFFECT

Somireddy Sreenivasa Reddy[1], K. Govardhan[2], Santoshi Misra[3] and G. Narender[4*]
[1]Department of Humanities and Science (Mathematics), Viganana Bharathi Institute of Technology, Hyderabad, Telangana, INDIA
[2]Department of Mathematics and Statistics, GITAM University, Hyderabad, Telangana, INDIA
[3]Department of Mathematics, Kaveri University, Gauraram (V), Wargal (M), Siddipet, Telangana, INDIA
[4]Department of Humanities and Sciences (Mathematics), CVR College of Engineering, Hyderabad, Telangana, INDIA
E-mail: gnriimc@gmail.com

A numerical investigation has been conducted on the 3D magnetohydrodynamic (MHD) flow of an incompressible Carreau fluid over a stretchable surface. Mathematical modeling is performed to represent the laws of conservation of mass, momentum, and heat transfer. An appropriate transformation transforms the governing partial differential equations (PDE) into the dimensionless ordinary differential equations (ODEs). To solve ODEs, we used the shooting technique with fourth order Adams-Moulton method implemented in a Fortran programming language. The validity of the computed results is established by benchmarking them against previously published findings in the literature. Key parameters influencing the flow are illustrated and discussed through graphical representations. The overall results indicate that the velocity profile diminishes with increasing magnetic parameter, while it increases in response to higher values of the Hall parameter and Weissenberg number. The fluid flow model examined in this study finds applications in nuclear reactor cooling systems, polymer extrusion processes, electromagnetic pumping, astrophysical plasma flows, and magnetohydrodynamic generators. Engineering and industrial quantities of interest, such as local skin friction and heat transfer rates, have been calculated and thoroughly discussed.

Key words: magnetohydrodynamic, thermal radiation, Carreau fluid, viscous dissipation, shooting technique.

Subject Classification Code: 35Q40,76D05

1. Introduction

Boundary layer problems involving a stretched surface have gained a lot of research attention in the last few decades due to the many applications associated with this topic that may be found in industrial and engineering processes. The concept of the boundary layer plays a crucial role in fluid mechanics and physics, where it is defined as the thin region of fluid near a surface where viscosity effects are dominant. Additionally, it is a location in the fluid flow where the fluid deforms with a relative velocity. Each main fluid has a few fundamental, significant characteristics that are crucial to its dynamics. In the manufacturing process, the rates of stretching and chilling are both important for the successful outcome of the finished product. Maintaining the stretching rate is crucial since a rapid shift in stretching might cause damage to the finished product due to abrupt solidification. Crane [1] was the first to describe the boundary layer-based, 2D flow of incompressible liquid along a stretched surface. Elbashbeshy [2] studied heat transfer analysis over a stretching surface, considering the effects of suction or injection. The fascinating fluid flow along a stretched sheet has been investigated by several researchers. [3, 4, 5].

Magneto signifies hydro, which means water, magnetic field, and dynamics implies movement. These three concepts are combined to form the term magnetohydrodynamics (MHD). The magnetic characteristics

* To whom correspondence should be addressed

of an electrically conducting fluid are examined via hydromagnetic flow. Also, magnetofluids, plasmas, liquid metals, seawater, and electrolytes are included. Engineering equipment like heat exchanger design, MHD electric power generators, and blood pumping machines are just a few examples of the many engineering uses for MHD flow. The introductory role of the magnetic constraint in the flow field is to create a resistive strength that maintains the flow and prevents boundary layer separation. The flow models that include hydromagnetic effects were studied by several researchers. Additionally, Pavlov [6] investigated the MHD flow of viscous fluids over a stretched surface. Electromagnetic hydrodynamic waves were proven to exist by Alfven [7]. Sarpakaya [8] investigated the movement of fluid types in magnetic fields.

Unsteady flows are those that rely on time. The time-dependent flow difficulties were looked at by Wang [9]. Moreover, some investigators examined the impact of a time-varying magnetic field force on flow inside the boundary flow regime. [10, 11, 12]. Ishak *et al.* [13] explored the emerging field of heat transport in a time-varying flow, casting new perspectives on this complex phenomenon. The generation of radiation due to temperature differences between the ambient fluid and its surroundings was a pivotal area of their study. Aziz [14] investigated the influence of Hall current on time-dependent heat transport, unveiling new findings that enhance our understanding of heat transfer. Furthermore, the research community has made significant progress in investigating the effects of radiative parameters [15, 16, 17], revealing new insights. Pal [18] studied the effects of hydromagnetic and Hall currents on irregular flow patterns.

Fluids classified as non-Newtonian fluids have complicated behaviour under stress and strain. Non-Newtonian fluids have also garnered a lot of interest in engineering and industry. Furthermore, a non-Newtonian Carreau fluid results from the coupling of a Newtonian fluid with a power law model. Actually, it is a particular type of Newtonian fluid whose viscosity property effects depend on both high and low shear rates. Narender *et al.* [19] examined the impacts of radiation, heat generation or absorption, and a magnetic field on the MHD Casson nanofluid flow over a radially stretching sheet. In a separate study, G. Narender *et al.* [20] examined the influences of external magnetic field inclinations with viscous dissipation resulting from heat generation / absorption on the mixed convective flow of the MHD Casson nanofluid, further adding to the importance of this research.

Recent progress in nanofluid research, particularly with advanced rheological models like Carreau fluids, has expanded opportunities for analyzing heat and mass transfer in complex systems. Irfan *et al.* [21] explored the role of thermal radiation in MHD Carreau nanofluids containing gyrotactic microorganisms, emphasizing energy-related applications and noting the significance of Soret-Dufour effects in coupled transport mechanisms. Building on this, Irfan *et al.* [22] performed a numerical investigation on nonlinear radiation and Joule heating within MHD bioconvective Carreau nanofluids, demonstrating that thermophoresis and Brownian motion exert contrasting influences on temperature and concentration profiles, while Peclet and bioconvection Lewis numbers reduce microbial density. Continuing along this line, Irfan *et al.* [23] examined nonlinear mixed convection in radiative Carreau nanofluids subject to Joule heating, activation energy, and Soret-Dufour effects. Their study showed that both thermo-Biot and Dufour numbers lead to higher temperature distributions, whereas Brownian motion diminishes temperature and concentration levels. In another study, Irfan and Muhammad [24] proposed a computational model for MHD radiative heat transfer in Carreau nanofluids with activation energy and cross-diffusion effects, revealing that thermal Biot and Dufour numbers increase heat transport, while Brownian motion acts to lower concentration fields.

Recent advances in nanofluid and non-Newtonian fluid modeling have expanded the scope of energy transport analysis. For example, Irfan [25] examined Joule heating and Arrhenius activation energy in Maxwell nanofluids, showing that heat sources and Eckert number enhance temperature, while Brownian motion and thermophoretic effects suppress heat transfer. Similarly, Irfan *et al.* [26] studied thermal transport in Carreau fluids under thermo-sloutal time's relaxation theory with variable conductivity and mass diffusivity, emphasizing the role of non-Fickian flux and relaxation times in accurately capturing thermal-mass transport behavior. Extending these ideas, Irfan *et al.* [27] evaluated a new mass flux theory on Carreau nanofluids, highlighting the contrasting effects of thermophoresis and Brownian motion on concentration profiles, alongside nonlinear convection impacts. These contributions complement the broader efforts in exploring coupled transport phenomena in complex fluids. The flow characteristics of a Carreau fluid along a stretched surface were shown by Hayat et al. [28]. Yusuf et al. [29] investigated MWCNT-Al_2O_3/water hybrid nanofluids and reported

enhanced heat transfer alongside reduced entropy generation in automotive radiator applications. In the field of solar energy, Bhatti et al. [30] found that manganese ferrite–nickel ferrite ferro-magnetic nanofluids strongly affect skin friction, pressure distribution, and thermal behavior, making them promising for improving the efficiency of solar nano-coatings. Furthermore, Bhatti et al. [31] explored magnetized nanofluid flow over a rotating disk in a non-Darcian porous medium and observed notable enhancements in flow, thermal, and mass transport characteristics, with implications for turbines, nuclear reactors, and biomedical technologies. Overall, these studies highlight that hybrid and magnetized nanofluids provide significant advantages in thermal management across automotive, renewable energy, and industrial systems. The surveyed research highlights the growing value of computational approaches in simulating biomedical processes. Umar et al. [32] demonstrated that the MWNNs-GAIPA framework effectively modeled the nonlinear dynamics of HIV prevention with high accuracy and stability. Shahzad et al. [33] emphasized the influence of nanoparticle geometry on heat transfer, reporting that platelet-shaped copper nanoparticles achieved the greatest thermal efficiency. In parallel, Waqas et al. [34] explored blood flow through stenotic arteries using gold–silver hybrid nanofluids, showing notable impacts on velocity, pressure, and temperature fields. Taken together, these studies underscore the promise of advanced numerical techniques in tackling complex problems related to disease dynamics, fluid flow, and biomedical applications. Recently, Bhatti et al. [30] modeled manganese ferrite/nickel ferrite ferro-magnetic hybrid nanofluids for solar nano-coatings, finding that magnetic and nanoparticle factors significantly affect skin friction, pressure, and temperature. Bhatti, Ellahi, and Sait [31] also examined magnetized nanofluid flow over a rotating disk, demonstrating that magnetic and thermal conditions strongly influence flow dynamics. Similarly, Yusuf et al. [29] investigated the heat transfer behavior of MWCNT-Al_2O_3 hybrid nanofluids, showing that higher nanoparticle concentrations enhance thermal efficiency and reduce entropy generation. Overall, these studies highlight the potential of hybrid and magnetic nanofluids to enhance heat transfer in modern thermal and energy systems.

This research extends the findings of [35] by adopting the Carreau fluid model as a replacement for the Casson fluid to capture more realistic rheological behavior. It investigates the combined effects of viscous dissipation and thermal radiation on unsteady stretching sheet flows, emphasizing their physical importance and engineering relevance. We will employ the shooting method with the Adams-Moulton method of order four to address the similarity equations obtained from the governing equations by similarity transformations. The organization of this article is structured as: Section 2 outlines the problem formulation, and the essential physical quantities of interest. In Section 3, we describe the application of the Adams-Moulton method to the proposed problem. Section 4 reviews the results, whereas Section 5 is reserved for concluding observations.

Novel contributions and significance of the study:

- To our knowledge, this study offers the framework of unsteady three-dimensional MHD flow of Carreau fluid over a stretching surface in which Hall current effects and radiative heat transfer are included.
- The research incorporates viscous dissipation hence enhancing their physical realism, and utility to actual thermal systems.
- This work obtains coupled ODEs from highly nonlinear governing PDEs through similar transformations and consequently, makes numerical analyses easier to perform.
- Employs an efficient numerical method which combines the shooting method with the fourth-order Adams-Moulton method to obtain accurate solutions to complicated fluid equations.
- Provides a comprehensive parametric analysis which covers the Weissenberg number, magnetic field strength, unsteadiness, Hall current, thermal radiation and viscous dissipation.
- This work computes engineering quantities such as skin friction and Nusselt number, thus furthering understanding of the thermal and momentum boundary layer behavior.
- Applicable to advanced technologies such as polymer extrusion, blood flow simulation, magnetic cooling systems, and MHD energy conversion systems

2. Mathematical modeling

An unsteady 3D, viscous, incompressible and Carreau fluid flow along a surface that is extended linearly. Subsequently, it is presumed that $y = 0$ indicating that the surface lies on the plane and the fluid is constrained to positive way of *y*-axis, and the liquid to be contained in the area where $y \geq 0$. Additionally, the sheet is thought to be stretched along the *x*-axis. We assume that a magnetic field is applied perpendicular to the sheet as illustrated in Fig.1.

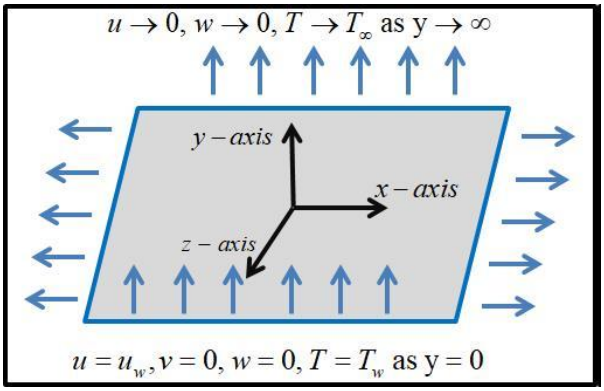


Fig.1. Configuration of the flow.

Being within the aforementioned limitations, the fundamental questions for the problem as modelled above are as follows [35]:

$$\partial(u_x) + \partial(u_y) + \partial(u_z) = 0, \tag{2.1}$$

$$\begin{aligned} &\partial(u_t) + u\,\partial(u_x) + v\,\partial(u_y) + w(u_z) = \\ &= \nu\left(1 + \frac{3(n-1)}{2}\Gamma^2\left[\partial(u_y)\right]^2\right)\left(\partial^2(u_{yy})\right) - \frac{\sigma B^2(t)}{\rho\left(1+m^2\right)}(u + mw), \end{aligned} \tag{2.2}$$

$$\begin{aligned} &\partial(w_t) + u\,\partial(w_x) + v\,\partial(w_y) + w\,\partial(w_z) = \\ &= \nu\left(1 + \frac{3(n-1)}{2}\Gamma^2\left(\partial(w_y)\right)^2\right)\left(\partial^2(w_{yy})\right) - \frac{\sigma B^2(t)}{\rho\left(1+m^2\right)}(mu - w), \end{aligned} \tag{2.3}$$

$$\partial(T_t) + u\,\partial(T_x) + v\,\partial(T_y) + w\,\partial(T_z) = \alpha_m\partial^2(T_{yy}) - \frac{1}{(\rho c_p)}\frac{\partial q_r}{\partial y} - \frac{\nu}{\rho}\left(\partial(u_y)\right)^2. \tag{2.4}$$

The associated BCs for the problem given by [35]:

$$\left.\begin{aligned} &u = u_w, \quad v = 0, \quad w = 0, \quad T = T_w \quad \text{when} \quad y = 0, \\ &u \to \infty, \quad w \to \infty, \quad T \to T_\infty, \quad y = 0, \ \text{when} \quad y \to \infty. \end{aligned}\right\} \tag{2.5}$$

In the above model, power-law index is taken as n, Γ is time constant, density by ρ, electrical conductivity by σ, the kinematic viscosity by ν, hall current by m, temperature taken as T, $\alpha_m = k/\rho\, c_p$ is thermal diffusivity, u_w the stretching velocity in $x-$direction, $u_w(x,t) = \dfrac{a\,x}{1-\gamma\,t}$ [28] is wall stretching velocity with time dependent and $B(t) = B_0\,(1-\gamma\,t)^{-\frac{1}{2}}$ is the magnetic field with time dependent where a and γ are constants.

The radiative heat flux vector can be described as [35]:

$$q_r = -\frac{4\sigma^*}{3\alpha^*}\,\partial\left(\left(T^4\right)_y\right) = -\frac{16\sigma^*}{3\alpha^*}T^3\,\partial\left(T_y\right). \tag{2.6}$$

The energy equation (2.4), on using (2.6) reduces to

$$\partial(T_t) + u\,\partial(T_x) + v\,\partial(T_y) + w\,\partial(T_z) = -\frac{\nu}{\rho}\left(\partial\left(u_y\right)\right)^2 + \partial\left(\left[\left(\alpha_m + \frac{16\sigma^* T^3}{3\alpha^*\rho c_p}\right)\partial\left(T_y\right)\right]_y\right). \tag{2.7}$$

Incorporating the stream function as given in Eq.(2.8), where represents the dimensionless variable, and are the non-dimensional velocity and temperature function in that order (see [35]).

$$\eta = y\sqrt{\frac{a}{\nu\,(1-\gamma\,t)}},\quad u = \frac{a\,x}{1-\gamma\,t}f_\eta\,(\eta),\quad v = -\sqrt{\frac{a\,\nu}{1-\gamma\,t}}\,f(\eta),$$

$$w = \frac{a\,x}{1-\gamma t}\,g(\eta) \quad \text{and} \quad T = T_\infty + \theta(\eta)\left[T_f - T_\infty\right]. \tag{2.8}$$

Considering Eq.(2.8) from model Eqs (2.1)-(2.4), the conservation of mass is validated. Using Eq.(2.8), the controlling Eqs (2.2)-(2.4) transform to these new equations.

$$\left(1 + \frac{3(n-1)}{2}We\left(f_{\eta\eta}\right)^2\right)f_{\eta\eta\eta} - \left(f_\eta\right)^2 + f\,f_{\eta\eta} - A\left(f_\eta + \frac{\eta}{2}f_{\eta\eta}\right) - \frac{M}{1+m^2}\left(f_\eta + m\,g\right) = 0. \tag{2.9}$$

$$\left(1 + \frac{3(n-1)}{2}We\left(f_{\eta\eta}\right)^2\right)g_{\eta\eta} + f\,g_\eta - g f_\eta - A\left(g + \frac{\eta}{2}g_\eta\right) + \frac{M}{1+m^2}\left(m\,f_\eta - g\right) = 0. \tag{2.10}$$

$$\left(1 + \frac{4}{3N_r}\left(1 + (tr-1)\theta\right)^3\right)\theta_{\eta\eta} - \Pr A\frac{\eta}{2}\theta_\eta + \Pr f\,\theta_\eta + \Pr\,Ec\left(f_{\eta\eta}\right)^2 +$$
$$+\left(\frac{4}{3N_r}(tr-1)\left(1+(tr-1)\theta\right)^2\right)\left(\theta_\eta\right)^2 = 0. \tag{2.11}$$

The transformed bounded constrained are:

$$\left.\begin{aligned} &\text{At} \quad \eta = 0: \quad f = 0, \quad f_\eta = 1, \quad g = 0, \quad \theta = 1, \\ &\text{As} \quad \eta \to \infty: \quad f_\eta \to 0, \quad g \to 0, \quad \theta \to 0 \end{aligned}\right\} \tag{2.12}$$

where prime is used for the derivative of unknown functions with respect to the similarity variable. The entrenched parameters are indicated as:

$$\begin{aligned} &A = \frac{\gamma}{a}, \quad Ec = \frac{a^2 x^2}{\alpha c_p \left(T_w - T_\infty\right)}, \quad M = \frac{\sigma B_0^2}{\rho a}, \quad N_r = \frac{k\alpha^*}{4\sigma^* T_\infty^3}, \quad \Pr = \frac{\nu}{\alpha_m}, \\ &tr = \frac{T_w}{T_\infty}, \quad We = \Gamma^2 \frac{a^3 x^2}{\nu\left(1-\gamma t\right)^2}. \end{aligned} \tag{2.13}$$

The technological quantities of interest are the wall friction and thermal gradients which specified as:

$$C_{fx} = \frac{\tau_{wx}}{\rho u_w^2}, \quad C_{fz} = \frac{\tau_{wz}}{\rho u_w^2}, \quad Nu_x = \frac{x q_w}{k\left(T_w - T_\infty\right)} \tag{2.14}$$

In the dimensionless form, the surface drag and Nusselt number are given by:

$$\left.\begin{aligned} &\sqrt{\mathrm{Re}_x}\, C_{fx} = \left(1 + \frac{(n-1)}{2} We \left(f''(0)\right)^2\right) f''(0), \\ &\sqrt{\mathrm{Re}_x}\, C_{fz} = \left(1 + \frac{(n-1)}{2} We \left(g'(0)\right)^2\right) g'(0), \\ &\frac{Nu_x}{\sqrt{\mathrm{Re}_x}} = -\left[1 + \frac{4}{3N_r}\left(1 + (t-1)\theta(0)\right)^3\right]\theta'(0). \end{aligned}\right\} \tag{2.15}$$

3. Method of solution

The solution methodology for the set of non-dimensional Eqs (2.9)-(2.11) and the wall conditions (2.12) modeling the problem is obtained using a numerical procedure with shooting techniques and the fourth-order Adams-Moulton method. This approach has been found to the effective for solving nonlinear differential equations with high accuracy. The set of coupled Eqs (2.9)-(2.10) with boundary conditions are solved separately by the shooting technique. In the future, the solution to Eqs (2.9)-(2.10) will be used in the Eq.(2.11) as a known input. Missing conditions $f''(0)$ and $g'(0)$ are to be chosen as r and s.
Furthermore, the following notations have been incorporated.

$$f = y_1, \quad f_\eta = y_2, \quad f_{\eta\eta} = y_3, \quad g = y_4, \quad g_\eta = y_5, \tag{3.1}$$

$$\frac{\partial f}{\partial r}=y_6,\quad \frac{\partial f_\eta}{\partial r}=y_7,\quad \frac{\partial f_{\eta\eta}}{\partial r}=y_8,\quad \frac{\partial g}{\partial r}=y_9,\quad \frac{\partial g_\eta}{\partial r}=y_{10},$$

$$\frac{\partial f}{\partial s}=y_{11},\quad \frac{\partial f_\eta'}{\partial s}=y_{12},\quad \frac{\partial f_{\eta\eta}}{\partial s}=y_{13},\quad \frac{\partial g}{\partial s}=y_{14},\quad \frac{\partial g_\eta}{\partial s}=y_{15}. \tag{3.1 cont.}$$

For simplification, the following notation has been defined.

$$1+\frac{3(n-1)}{2}We(y_3)^2=\phi_1,\quad 1+\frac{3(n-1)}{2}We(y_5)^2=\phi_2. \tag{3.2}$$

The following system of ODE is obtained:

$$y_1'=y_2, \qquad y_1(0)=0,$$

$$y_2'=y_3, \qquad y_2(0)=1,$$

$$y_3'=\frac{1}{\phi_1}\left[A\left(y_2+\frac{\eta}{2}y_3\right)-y_1y_3+y_2^2+\frac{M}{1+m^2}(y_2+my_4)\right], \qquad y_3(0)=r,$$

$$y_4'=y_5, \qquad y_4(0)=0,$$

$$y_5'=\frac{1}{\phi_2}\left[A\left(y_4+\frac{\eta}{2}y_5\right)+y_4y_2-y_1y_5-\frac{M}{1+m^2}(my_2-y_4)\right], \qquad y_5(0)=s,$$

$$y_6'=y_7, \qquad y_6(0)=0,$$

$$y_7'=y_8, \qquad y_7(0)=0,$$

$$y_8'=\frac{1}{\phi_1^2}\left\{\phi_1\left[A\left(y_7+\frac{\eta}{2}y_8\right)-h_1y_8-h_3y_6+2y_2y_7+\frac{M}{1+m^2}(y_7+my_9)\right]+\right.$$
$$\left.+\left[A\left(y_2+\frac{\eta}{2}y_3\right)-y_1y_3+y_2^2+\frac{M}{1+m^2}(y_2+my_4)\right]3(n-1)Wey_3y_8\right\}, \qquad h_8(0)=1,$$

$$y_9'=y_{10}, \qquad y_9(0)=0,$$

$$y_{10}'=\frac{1}{\phi_2^2}\left\{\phi_2\left[A\left(y_9+\frac{\eta}{2}y_{10}\right)+y_4y_7+y_9y_2-y_1y_{10}-y_6y_5-\frac{M}{1+m^2}(my_7-y_9)\right]+\right.$$
$$\left.+\left[A\left(y_4+\frac{\eta}{2}y_5\right)+y_4y_2-y_1y_5-\frac{M}{1+m^2}(my_2-y_4)\right]3(n-1)We\,y_5y_{10}\right\}, \qquad y_{10}(0)=0,$$

$$y_{11}' = y_{12}, \qquad y_{11}(0) = 0,$$

$$y_{12}' = y_{13}, \qquad y_{12}(0) = 0,$$

$$y_{13}' = \frac{1}{\phi_1^2}\left\{\phi_1\left[A\left(y_{12} + \frac{\eta}{2}y_{13}\right) - y_1 y_{13} - y_3 y_{11} + 2y_2 y_{12} + \frac{M}{1+m^2}\left(y_{12} + m y_{14}\right)\right] + \right.$$
$$\left. + \left[A\left(y_2 + \frac{\eta}{2}y_3\right) - y_1 y_3 + y_2^2 + \frac{M}{1+m^2}\left(y_2 + m y_4\right)\right] 3(n-1)We\, y_3 y_{12}\right\}, \qquad h_{14}(0) = 0,$$

$$y_{14}' = y_{15}, \qquad y_{14}(0) = 0,$$

$$y_{15}' = \frac{1}{\phi_2^2}\left\{\phi_2\left[A\left(y_{14} + \frac{\eta}{2}y_{15}\right) + y_4 y_{12} + y_{14} y_2 - y_1 y_{15} - y_{11} y_5 + \right.\right.$$
$$\left. - \frac{M}{1+m^2}\left(m y_{12} - y_{14}\right)\right] + \left[A\left(y_4 + \frac{\eta}{2}y_5\right) + y_4 y_2 - y_1 y_5 - \frac{M}{1+m^2}\left(m y_2 - y_4\right)\right] \times \qquad y_{15}(0) = 1,$$
$$\left. \times + 3(n-1)We\, y_5 y_{10}\right\}.$$

The above IVP is solved by employing Adams-Moulton method for initial choice of r and s. The domain of problem is considered to be bounded i.e. $[0, \eta_{\max}]$. The initial missing conditions (ICs) must be chosen in the above IVP so that:

$$y_2(\eta_\infty, r, s) = 0, \qquad y_4(\eta_\infty, r, s) = 0\,. \tag{3.3}$$

Newton's iterative approach is utilized to improve the missing initial condition, following the procedure outlined here.

$$\begin{pmatrix} r^{k+1} \\ s^{k+1} \end{pmatrix} = \begin{pmatrix} r^k \\ s^k \end{pmatrix} - \begin{pmatrix} y_7 & y_9 \\ y_{11} & y_{14} \end{pmatrix}^{-1} \begin{pmatrix} y_2 \\ y \end{pmatrix}_{\left(r^k, s^k, \eta\right)}, \tag{3.4}$$

The completion of the shooting technique requires the following steps.

(i) Selecting the values $r = r^{(0)}$ and $s = s^{(0)}$.

(ii) Choose $\varepsilon > 0$.

If $\max\left\{\left|y_2(\eta_\infty) - 0\right|, \left|y_4(\eta_\infty) - 0\right|\right\} < \varepsilon$, stop, or else go to (iii).

(iii) Calculate $r^{(k+1)}$ and $s^{(k+1)}$, $k = 0, 1, 2, \ldots\ldots\ldots$, using (3.4).

(iv) Do again (i) in addition (ii).

All through this article, ε has been taken as $\varepsilon = 10^{-4}$. The choice of $\eta_{\max} = 7$ was more than enough for end condition.

Similarly, by treating f as a known function, it is possible to solve the ODE (2.11) and the accompanying BCs.

4. Representation of graphs and tables

It has been given and examined how the dimensionless mathematical model can be solved numerically. In this analysis, the shooting method combined with the Adams-Moulton method has been chosen to reproduce the solution from [35]. A thorough discussion on the graphs and tables has been conducted which contains the effects of dimensionless parameters on velocity behavior, the temperature profile, the skin friction and Nusselt number. To ensure the reliability of the results, the currently obtained outcomes are compared with solutions available in previously published literature. From Tabs 1 and 2, it can be concluded that the results show strong consistency with previously published results.

Table 1, explains the impact of magnetic parameter, Hall current m, unsteadiness, Weissenberg number and power law-index on the skin friction $-C_{fx}\,\mathrm{Re}^{1/2}$ and $-C_{fz}\,\mathrm{Re}^{1/2}$. The value $n=3$ is fixed throughout the discussion. Further, the increasing values of M, the skin friction coefficients rise in both directions. Due to rising values of Hall current, $-C_{fx}\,\mathrm{Re}^{1/2}$ are reduced while, $-C_{fz}\,\mathrm{Re}^{1/2}$ is increases. By ascending values of unsteadiness A, there is a marginal increase in skin friction along both directions x, z. Meanwhile, due to extending the values of Weissenberg number, skin friction along x direction is increased and a marginal increment along z direction is seen.

Tab.1. Comparison of the present results of $-C_{fx}\,\mathrm{Re}^{1/2}$ and $-C_{fz}\,\mathrm{Re}^{1/2}$ with different values of M, m, A and We.

M	m	A	We	$-C_{fx}\,\mathrm{Re}^{1/2}$		$-C_{fz}\,\mathrm{Re}^{1/2}$	
				[35]	**Present**	**[35]**	**Present**
0.5	*0.1*	*0.1*	*0.05*	*1.27682813*	*1.276832000*	*0.02280321*	*0.02280094*
1				*1.47275246*	*1.472753000*	*0.03841592*	*0.03841573*
1.13				*1.52006638*	*1.520066000*	*0.04188206*	*0.04188195*
	0.5			*1.24036080*	*1.240361000*	*0.09561976*	*0.09560762*
	1.0			*1.17768745*	*1.177676000*	*0.12810130*	*0.1280709*
		0.2		*1.30688119*	*1.306885000*	*0.02219995*	*0.022198130*
		0.3		*1.33663405*	*1.336637000*	*0.02161821*	*0.021617010*
			0.1	*1.29858276*	*1.298587000*	*0.02300580*	*0.023003560*
			0.15	*1.31813375*	*1.318137000*	*0.02318507*	*0.023182880*

In Tab.2, the effects of the M, m, A, Nr, We, and Pr on Nusselt number $Nu_x\,\mathrm{Re}^{-1/2}$ discussed. The rising pattern is noticed in the $Nu_x\,\mathrm{Re}^{-1/2}$ due to the extending quantities of Hall current, Prandtl number and temperature ratio, whereas Nusselt number decreases due to accelerating values of magnetic parameter, unsteadiness parameter and radiation parameter.

Figures 2-4 show how variations in the magnetic field parameter affect velocity and temperature profiles. An increase in this parameter causes a decrease in velocity along the *x*-direction, while velocity in the perpendicular (*z*) direction rises, accompanied by a gradual increase in temperature. This parameter quantifies the Lorentz force exerted on the electrically conducting micropolar nanofluid, which acts as a resistive force when the moving fluid interacts with a magnetic field. As the magnetic field parameter increases, the Lorentz force strengthens, opposing the primary flow and reducing velocity in the *x*-direction while enhancing

secondary flow components. The additional energy dissipation from this interaction also elevates the temperature profile, which is relevant for thermal management in magnetohydrodynamic (MHD) systems such as nuclear reactor cooling and MHD power generation.

Tab.2. Data comparing the numerical results of the $Nu_x \, \mathrm{Re}^{-1/2}$ with different values of M, m, A, Nr, We, and Pr.

M	m	A	Nr	We	Pr	$Nu_x \, \mathrm{Re}^{-1/2}$	
						[35]	Present
0.5	*0.1*	*0.1*	*2*	*0.05*	*10*	*2.71034759*	*2.664940000*
1						*2.64150549*	*2.588308000*
1.13						*2.62506716*	*2.570028000*
	0.5					*2.72241537*	*2.678329000*
	1.0					*2.74397741*	*2.702283000*
		0.2				*2.70211916*	*2.574201000*
		0.3				*2.69394188*	*2.426289000*
			4			*2.47075201*	*2.467486000*
			6			*2.38156287*	*2.378252000*
				0.1		*2.72299927*	*2.719883000*
				0.15		*2.73378326*	*2.730636000*
					15	*3.92330151*	*3.424953000*
					20	*4.03600482*	*4.029062000*

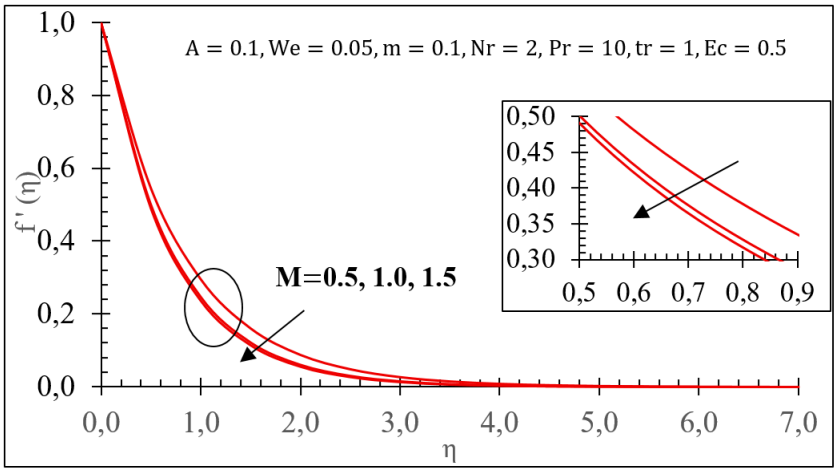


Fig.2. Variation in $f^{''}(\eta)$.

Figures 5-7 present the influence of the Hall parameter on velocity and temperature distributions. Higher values of the Hall parameter result in an increase in velocity along the *x*-direction, a slight rise in velocity along the *z*-direction, and a minor decrease in temperature. This effect occurs because the Hall current becomes prominent under strong magnetic fields, originating from the transverse motion of charged particles within the conducting fluid. Such behavior alters both flow patterns and heat transfer characteristics, which is important for practical applications in engineering, including plasma flows, MHD generators, and electromagnetic pumps, where Hall effects can be leveraged to enhance efficiency.

Figures 8-10 present the impact of the unsteadiness parameter (A) on the velocity and temperature distributions. Figure 8 shows that increasing unsteadiness produces a slight enhancement in velocity along the

x-direction. This behavior is attributed to time-dependent acceleration effects, which strengthen fluid motion in this direction.

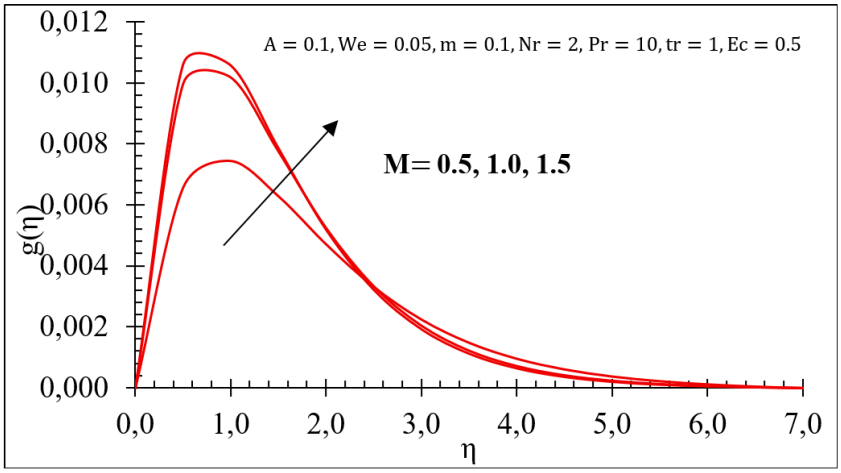


Fig.3. Variation in $g(\eta)$.

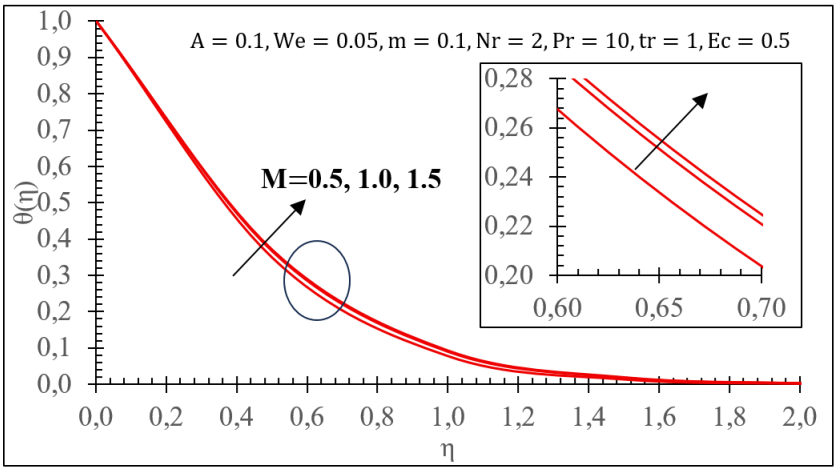


Fig.4. Variation in temperature behaviour $\theta(\eta)$.

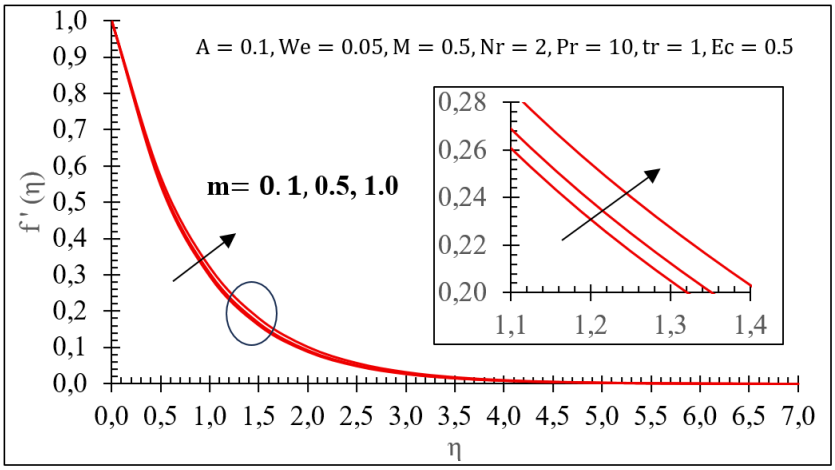


Fig.5. Variation in $f''(\eta)$.

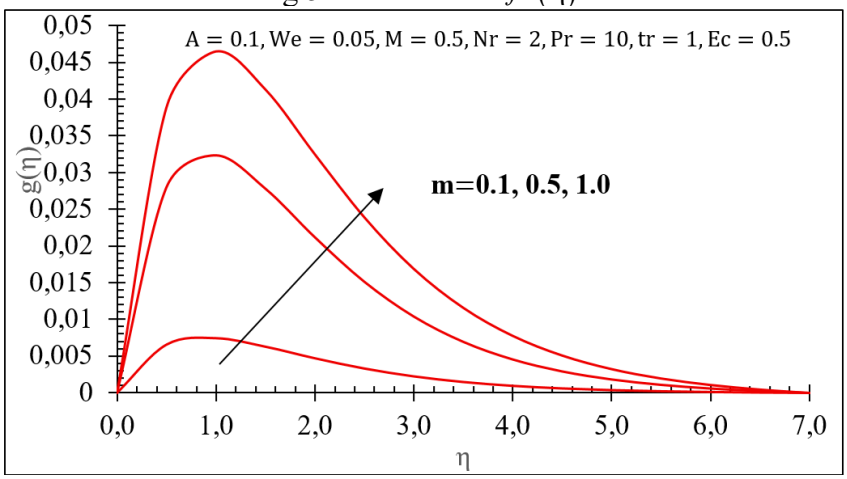


Fig.6. Variation in $g(\eta)$.

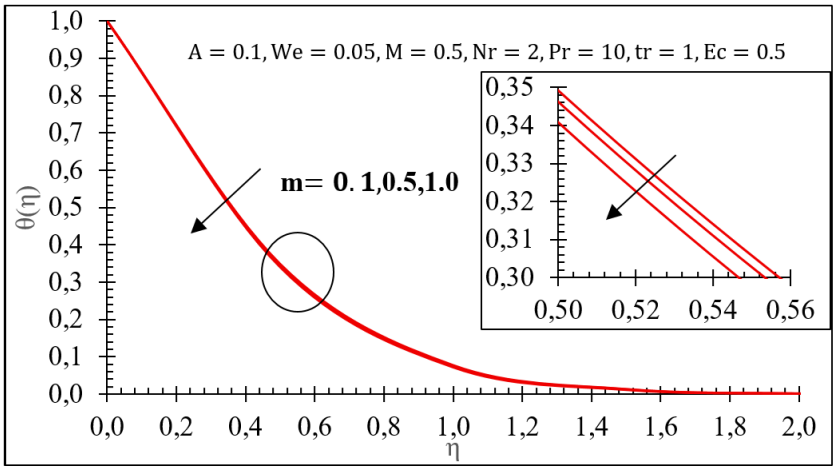


Fig.7. Variation in temperature behaviour $\theta(\eta)$.

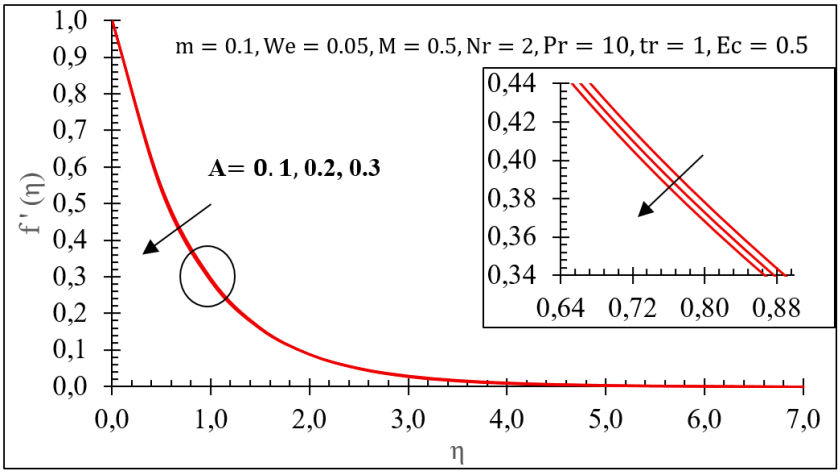


Fig.8. Variation in $f''(\eta)$.

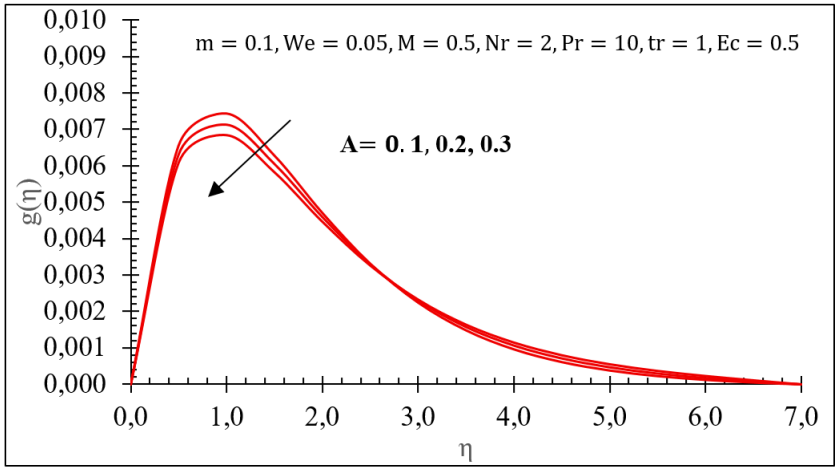


Fig.9. Variation in $g(\eta)$.

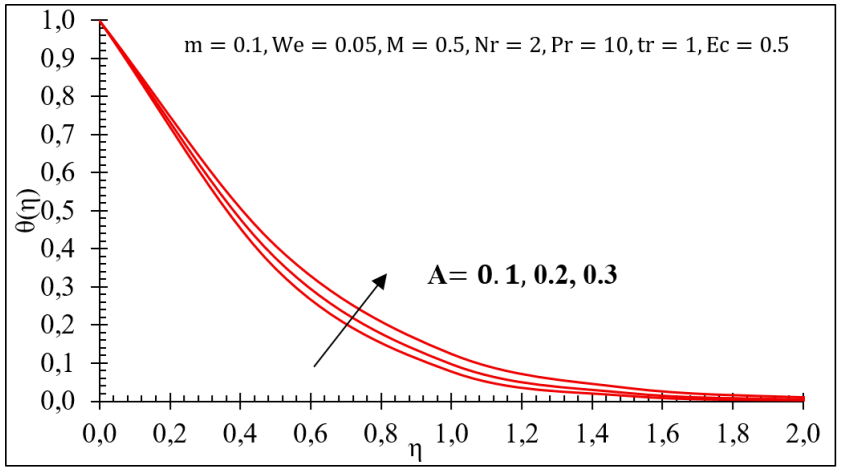


Fig.10. Variation in temperature behaviour $\theta(\eta)$.

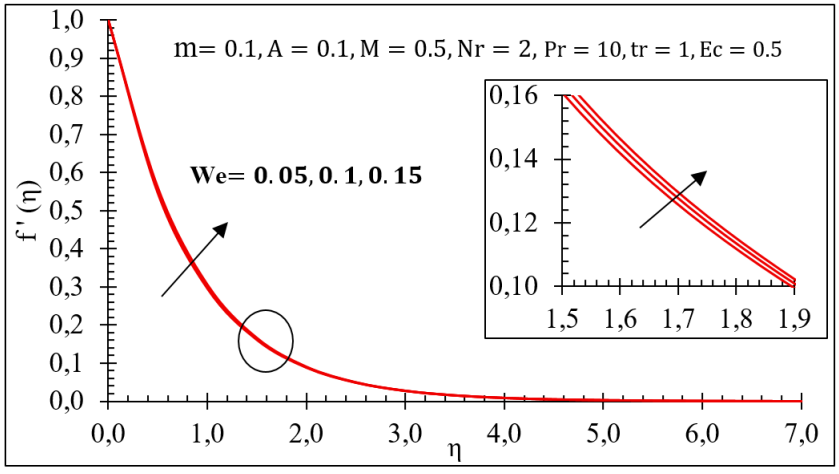


Fig.11. Variation in $f''(\eta)$.

In contrast, Fig.9 indicates a reduction in velocity along the *z*-direction with higher unsteadiness, due to temporal variations that hinder momentum transfer in that orientation. Figure 10 demonstrates that the temperature profile rises with increasing unsteadiness. This can be physically explained by the fact that unsteadiness amplifies convective heat transport, leading to greater thermal energy retention within the boundary layer. Practically, adjusting the unsteadiness parameter offers a way to control both flow patterns and heat transfer rates, which is important in applications such as unsteady cooling processes, pulsatile flows, and thermal regulation in rotating equipment.

Figures 11-13 depict how variations in the Weissenberg number (*We*) affect the velocity and temperature distributions. As shown in Figures 11 and 12, an increase in *We* results in a slight decline in velocity within the boundary layer. This occurs because the Weissenberg number represents the relative contribution of fluid elasticity arising from the relaxation time constant in comparison to viscous effects. Higher values enhance elastic forces, which tend to resist the flow and slightly reduce velocity. Figure 13 shows that the temperature profile increases modestly with rising *We*. This can be attributed to increased elastic effects, which enhance internal energy dissipation and thus expand the thermal boundary layer. From a practical perspective, adjusting the Weissenberg number offers a means to control both flow resistance and heat transfer, which is particularly relevant in engineering systems involving non-Newtonian fluids, such as polymer processing, lubrication technologies, and thermal management in heat exchangers.

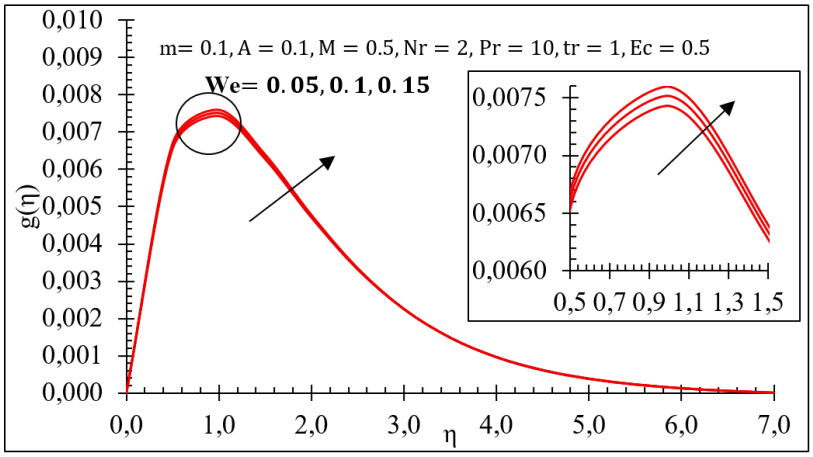


Fig.12. Variation in $g(\eta)$.

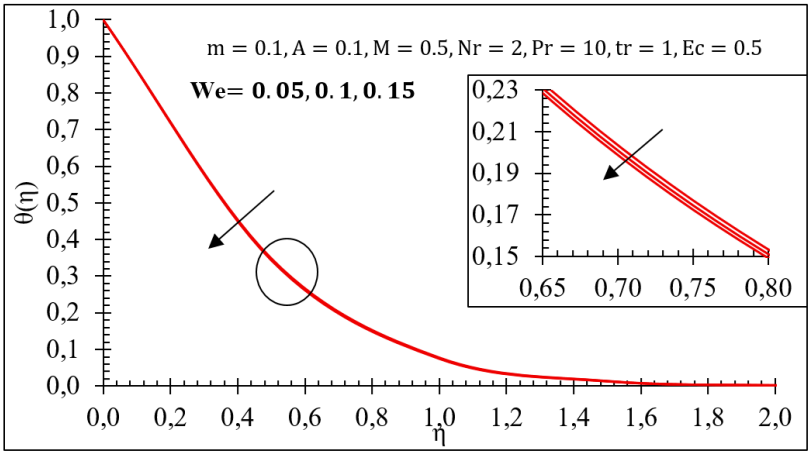


Fig.13. Variation in temperature behaviour $\theta(\eta)$.

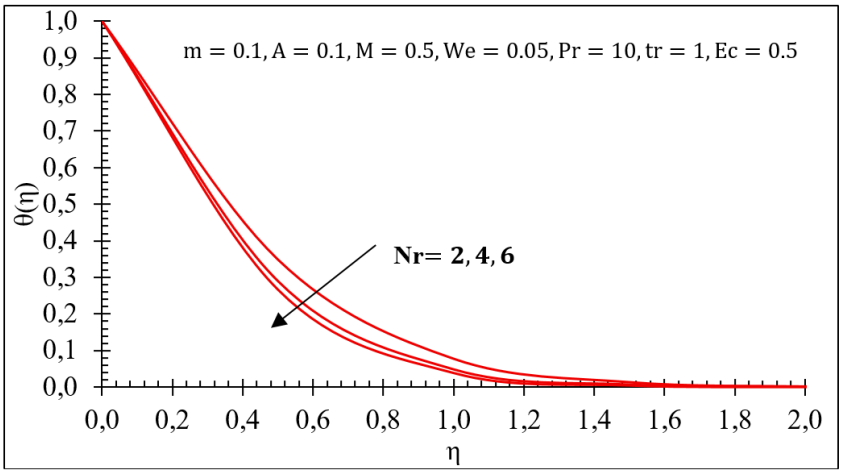


Fig.14. Variation in temperature behaviour $\theta(\eta)$.

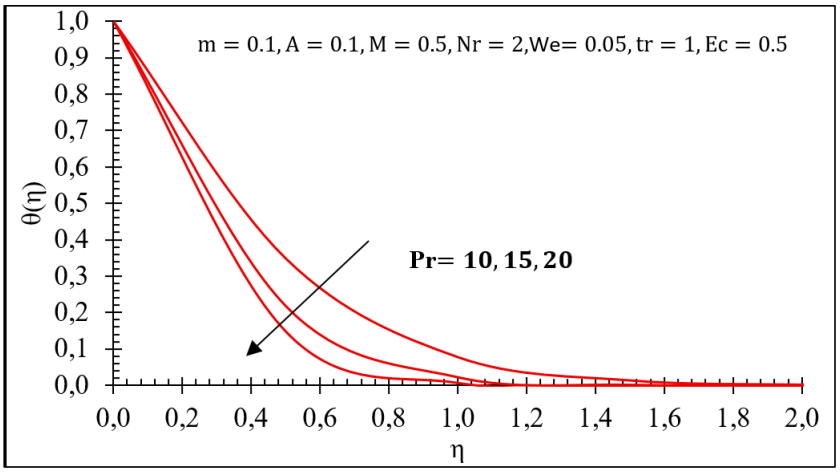


Fig.15. Variation in temperature behaviour $\theta(\eta)$.

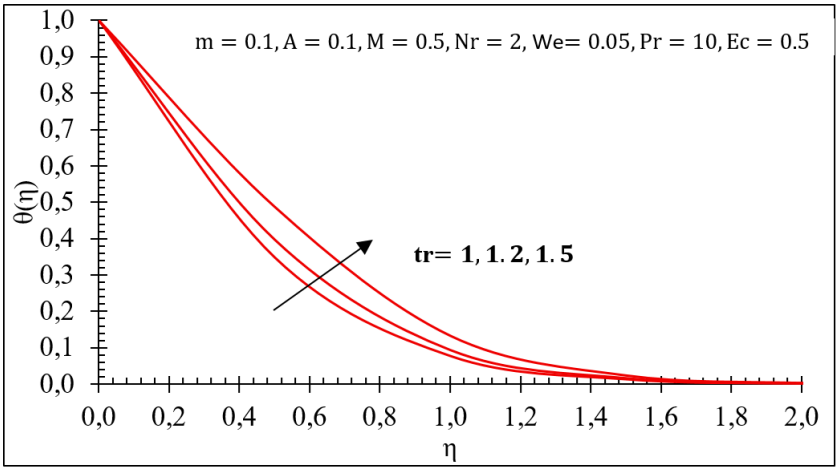


Fig.16. Variation in temperature behaviour $\theta(\eta)$.

Figures 14-16 illustrate how the temperature profile within the boundary layer is influenced by the radiation parameter (Nr), Prandtl number (Pr), and temperature ratio (tr). As shown in Figs 14 and 15, increasing either Nr or Pr causes a marked decrease in temperature. This can be explained physically: a higher Prandtl number reflects an increase in momentum diffusivity relative to thermal diffusivity, which limits heat penetration and reduces the thickness of the thermal boundary layer. Fluids with elevated Pr values therefore conduct momentum more effectively than heat, a property beneficial for systems where precise thermal regulation is required, such as advanced cooling technologies. Similarly, a rise in the radiation parameter amplifies radiative heat loss, thereby lowering the fluid temperature a factor of significance in systems where radiative effects dominate, such as in solar energy applications or high-temperature thermal coatings. In contrast, Fig.16 demonstrates that increasing the temperature ratio (tr) leads to a broader temperature distribution within the boundary layer. This effect arises from a larger temperature difference between the surface and surrounding fluid, which intensifies thermal driving forces and facilitates deeper heat penetration. Such behavior has important practical implications, indicating that controlling the temperature ratio offers an effective approach to optimizing heat transfer in engineering devices like heat exchangers, energy conversion systems, and thermal coating applications.

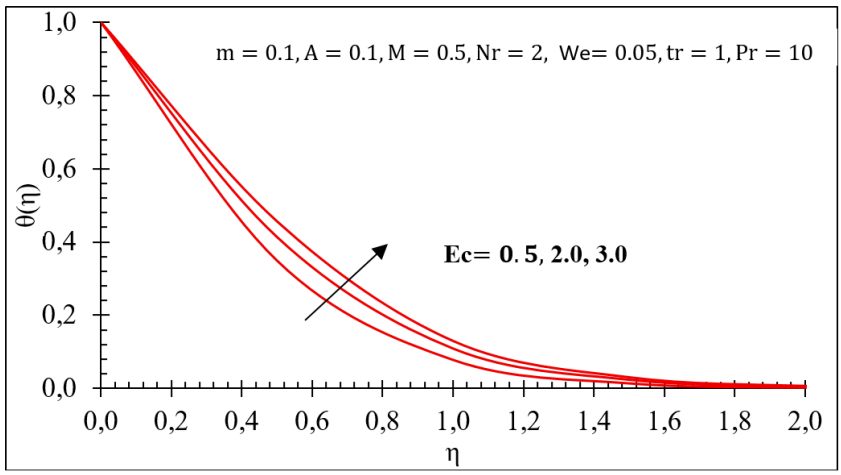


Fig.17. Variation in temperature behaviour $\theta(\eta)$.

Figure 17 illustrates how Ec effects on $\theta(\eta)$. As Ec is boosted, heat transmission increases. The viscous dissipation effect is measured by Eckert number, which is the ratio between thermal energy transported into or out of the fluid to the kinetic energy lost during flow. This graph shows how the temperature distribution profile rises in tandem with the temperature profile's Eckert number values.

5. Conclusion

The model equations are transformed from the initial partial derivatives to ordinary derivatives and solved using the numerical approach of shooting with the Adams Moulton method. The numerical outcomes are displayed using figures and tables with appropriate deliberations of results relevant to various applications. The solutions to the model equations compared favorably with existing studies in the limiting sense. To analyze the influence of several physical parameters on velocity and temperature the results are presented and explained through comprehensive graphs and tables. The study concludes with several noteworthy findings, offering insights into the behavior of MHD Carreau fluid flows under different conditions. From the current numerical study, the following essential outcomes are outlined:

- The effect of the Weissenberg number on both velocity and temperature is not very prominent. Even so, a small rise in temperature occurs as a result of the fluid's elastic nature, while the velocity shows a minor decline because of the greater resistance to deformation.
- As the magnetic parameter increases, the velocity along the *x*-axis decreases, reflecting the enhanced resistive effects that hinder the fluid's motion and reduce the flow rate.
- Increasing the Hall current enhances velocity along the *z*-axis and slightly in the transverse direction, while slightly reducing the Carreau fluid's temperature.
- As unsteadiness (A) rises, the overall velocity decreases because of the fluctuating flow, while the velocity along the *x*-axis of the Carreau fluid shows little change.
- Rising unsteadiness (A) results in higher temperatures in the Carreau fluid, suggesting that intensified flow fluctuations enhance heat transfer within the fluid.
- $-C_{fx}\,\mathrm{Re}^{1/2}$ and $-C_{fz}\,\mathrm{Re}^{1/2}$, show strong links between thermal and momentum effects affected by important physical parameters.

Acknowledgements

The authors acknowledge the constructive suggestions received from the reviewers and the editor which led to definite improvements in the paper.

Nomenclature

A – unsteadiness parameter
$B(t)$ – time-dependent magnetic field
C_{fx} – skin friction coefficient in *x* direction
C_{fz} – skin friction coefficient in *z* direction
f^1, g – dimensionless velocity in x and z direction
M – magnetic parameter
m – Hall current parameter
n – power law-index
Nr – radiation parameter
Nu_x – local Nusselt number

Pr – Prandtl number
q_w – wall heat transfer coefficient
T – temperature of the fluid
T_w – fluid temperature at the surface
T_∞ – fluid temperature at infinity
tr – temperature ratio parameter
u, v, w – velocity component in x, y and z directions
We – Weissenberg number
α^* – Rosseland mean absorption coefficient
α_m – thermal diffusivity of the fluid
β – Casson fluid parameter
Γ – time constant
η – dimensionless similarity variable
θ – dimensionless fluid temperature
κ – thermal conductivity of the fluid
υ – kinematic viscosity of the fluid
ρ – density of the fluid
σ – electrical conductivity of the fluid
σ^* – Stefan-Boltzmann constant
τ_{wz} – shear stress component in z direction
τ_{wx} – shear stress component in x direction
Υ, a – constant

References

[1] Crane L.J. (1970): *Flow past a stretching plate*.– Zeitschrift für Angewandte Mathematik und Physik, vol.21, No.4, pp.645-647, https://doi.org/10.1007/BF01587695.

[2] Elbashbeshy E.M. (1998): *Heat transfer over a stretching surface with variable surface heat flux*.– Journal of Physics D: Applied Physics, vol.31, No.16, pp.1951-1954, https://doi.org/10.1088/0022-3727/31/16/002.

[3] Mahapatra T.R. and Gupta A. (2002): *Heat transfer in stagnation-point flow towards a stretching sheet*.– Heat and Mass Transfer, vol.38, No.6, pp.517-521, https://doi.org/10.1007/s002310100215.

[4] Salleh M.Z., Nazar R. and Pop I. (2010): *Boundary layer flow and heat transfer over a stretching sheet with Newtonian heating*.– Journal of the Taiwan Institute of Chemical Engineers, vol.41, No.6, pp.651-655, https://doi.org/10.1016/j.jtice.2010.01.013.

[5] Misra M., Ahmad N. and Siddiqui Z.U. (2012): *Unsteady boundary layer flow past a stretching plate and heat transfer with variable thermal conductivity*.– World Journal of Mechanics, vol.2, No.1, pp.35-41, https://doi.org/10.4236/wjm.2012.21005.

[6] Pavlov K. (1974): *Magnetohydrodynamic flow of an incompressible viscous fluid caused by deformation of a plane surface*.– Magnitnaya Gidrodinamika, vol.4, No.1, pp.146-147

[7] Alfven H. (1942): *Existence of electromagnetic-hydrodynamic waves*.– Nature, vol.150, No.3805, pp.405-406, https://doi.org/10.1038/150405d0.

[8] Sarpkaya T. (1961): *Flow of non-Newtonian fluids in a magnetic field*.– AIChE Journal, vol.7, No.2, pp.324-328, https://doi.org/10.1002/aic.690070231.

[9] Wang C. (1990): *Liquid film on an unsteady stretching surface*.– Quarterly Journal of Applied Mathematics, vol.48, No.4, pp.601-610, https://doi.org/10.1090/qam/1079908.

[10] Takhar H., Chamkha A. and Nath G. (1999): *Unsteady flow and heat transfer on a semi-infinite plate with an aligned magnetic field*.– International Journal of Engineering Science, vol.37, No.13, pp.1723-1736, https://doi.org/10.1016/S0020-7225(98)00142-9.

[11] Chamkha A.J. and Al-Mudhaf A. (2005): *Unsteady heat and mass transfer from a rotating vertical cone with a magnetic field and heat generation or absorption effects*.– International Journal of Thermal Sciences, vol.44, No.3, pp.267-276, https://doi.org/10.1016/j.ijthermalsci.2004.06.005.

[12] Chamkha A.J. and Ahmed S. (2011): *Similarity solution for unsteady MHD flow near a stagnation point of a three-dimensional porous body with heat and mass transfer, heat generation/absorption and chemical reaction*.– Journal of Applied Fluid Mechanics, vol.4, No.2, pp.87-99, https://doi.org/10.36884/jafm.4.02.19131.

[13] Ishak A., Nazar R. and Pop I. (2009): *Boundary layer flow and heat transfer over an unsteady stretching vertical surface*.– Meccanica, vol.44, No.4, pp.369-375, https://doi.org/10.1007/s11012-008-9176-9.

[14] El-Aziz M.A. (2010): *Flow and heat transfer over an unsteady stretching surface with Hall effect*.– Meccanica, vol.45, No.1, pp.97-109, https://doi.org/10.1007/s11012-009-9227-x.

[15] Chamkha A.J. (2001): *Coupled heat and mass transfer by natural convection about a truncated cone in the presence of magnetic field and radiation effects*.– Numerical Heat Transfer: Part A: Applications, vol.39, No.5, pp.511-530, https://doi.org/10.1080/104077801300140228.

[16] El-Aziz M.A. (2009): *Radiation effect on the flow and heat transfer over an unsteady stretching sheet*.– International Communications in Heat and Mass Transfer, vol.36, No.5, pp.521-524, https://doi.org/10.1016/j.icheatmasstransfer.2009.02.001.

[17] Rashidi M. and Abbasbandy S. (2011): *Analytic approximate solutions for heat transfer of a micropolar fluid through a porous medium with radiation*.– Communications in Nonlinear Science and Numerical Simulation, vol.16, No.4, pp.1874-1889, https://doi.org/10.1016/j.cnsns.2010.08.016.

[18] Pal D. (2013): *Hall current and MHD effects on heat transfer over an unsteady stretching permeable surface with thermal radiation*.– Computers & Mathematics with Applications, vol.66, No.7, pp.1161-1180, https://doi.org/10.1016/j.camwa.2013.07.012.

[19] Narender G., Govardhan K. and Sreedhar Sarma G. (2020): *Magnetohydrodynamic stagnation point on a Casson nanofluid flow over a radially stretching sheet*.– Beilstein Journal of Nanotechnology, vol.11, pp.1303-1315, https://doi.org/10.3762/bjnano.11.114.

[20] Narender G., Govardhan K. and Sreedhar Sarma G. (2021): *MHD Casson nanofluid past a stretching sheet with the effects of viscous dissipation, chemical reaction and heat source/sink*.– Journal of Applied and Computational Mechanics, vol.7, No.4, pp.2040-2048, https://doi.org/10.22055/jacm.2021.37803.3087.

[21] Irfan M., Alasiri A., Khan M. and Anwar M.S. (2025): *Thermal radiation optimization in magnetohydrodynamic Carreau nanofluids with gyrotactic microorganisms for energy applications*.– Journal of Radiation Research and Applied Sciences, vol.18, No.3, 101809, https://doi.org/10.1016/j.jrras.2025.101809.

[22] Irfan M., Muhammad T., Rashid M., Anwar M.S., Abas S.S. and Satya Narayana P.V. (2025): *Numerical study of nonlinear thermal radiation and Joule heating on MHD bioconvection Carreau nanofluid with gyrotactic microorganisms*.– Journal of Radiation Research and Applied Sciences, vol.18, No.1, 101254, https://doi.org/10.1016/j.jrras.2024.101254.

[23] Irfan M., Anwar M.S., Kebail I. and Khan W.A. (2023): *Thermal study on the performance of Joule heating and Soret–Dufour influence on nonlinear mixed convection radiative flow of Carreau nanofluid*.– Tribology International, vol.188, 108789, https://doi.org/10.1016/j.triboint.2023.108789.

[24] Irfan M. and Muhammad T. (2024): *Computational framework of MHD radiative heat transfer to Carreau nanofluid with Soret-Dufour effects and activation energy*.– ZAMM - Journal of Applied Mathematics and Mechanics, vol.104, No.3, e202300410, https://doi.org/10.1002/zamm.202300410.

[25] Irfan M. (2023): *Energy transport phenomenon via Joule heating and aspects of Arrhenius activation energy in Maxwell nanofluid*.– Waves in Random and Complex Media, pp.1-16, https://doi.org/10.1080/17455030.2023.2196348.

[26] Irfan M., Anwar M.S., Sardar H., Khan M. and Khan W.A. (2022): *Energy transport and effectiveness of thermo-solutal time's relaxation theory in Carreau fluid with variable mass diffusivity*.– Mathematical Problems in Engineering, vol.2022, 8208342, https://doi.org/10.1155/2022/8208342.

[27] Irfan M., Rafiq K., Anwar M.S., Sajjad R., Khan M. and Khan W.A. (2021): *Evaluating the performance of new mass flux theory on Carreau nanofluid using the thermal aspects of convective heat transport*.– Pramana - Journal of Physics, vol.95, No.4, 203, https://doi.org/10.1007/s12043-021-02217-7.

[28] Hayat T., Asad S., Mustafa M. and Alsaedi A. (2014): *Boundary layer flow of Carreau fluid over a convectively heated stretching sheet*.– Applied Mathematics and Computation, vol.246, pp.12-22, https://doi.org/10.1016/j.amc.2014.07.116.

[29] Yusuf A., Khan S.U., Hassan M., Nofal T.A., Al-Mulla A. and Abd-Alla A.M. (2025): *Heat transfer optimization of MWCNT-Al_2O_3 hybrid nanofluids under convective and irreversible effects*.– Journal of Umm Al-Qura University for Applied Sciences, https://doi.org/10.1007/s43994-025-00252-3.

[30] Bhatti M.M., Bég O.A., Khalique C.M., Zeeshan A. and Sait S.M. (2025): *Computation of manganese ferrite/nickel ferrite ethylene glycol hybrid ferro-magnetic nanofluid stretching flow with radiative flux: Applications in solar nano-coatings*.– The European Physical Journal Special Topics, https://doi.org/10.1140/epjs/s11734-025-01742-5.

[31] Bhatti M.M., Ellahi R. and Sait S.M. (2025): *Numerical investigation of magnetized nanofluid flow in a non-Darcian medium with convective heating conditions across a rotating disk*.– International Journal of Numerical Methods for Heat & Fluid Flow, vol.35, No.5, pp.1736-1763, https://doi.org/10.1108/HFF-03-2025-0135.

[32] Umar M., Amin F., Al-Mdallal Q. and Ali M.R. (2022): *A stochastic computing procedure to solve the dynamics of prevention in HIV system*.– Biomedical Signal Processing and Control, vol.78, 103888, https://doi.org/10.1016/j.bspc.2022.103888.

[33] Shahzad A., Liaqat F., Ellahi Z., Rahman S., Bukhari S.M. and Gulzar M.M. (2022): *Thin film flow and heat transfer of Cu-nanofluids with slip and convective boundary condition over a stretching sheet*.– Scientific Reports, vol.12, 14254, https://doi.org/10.1038/s41598-022-18049-3.

[34] Waqas H., Farooq U., Hassan A., Liu D., Noreen S., Makki R., Imran M. and Ali M.R. (2023): *Numerical and computational simulation of blood flow on hybrid nanofluid with heat transfer through a stenotic artery: Silver and gold nanoparticles*.– Results in Physics, vol.44, 106152, https://doi.org/10.1016/j.rinp.2022.106152.

[35] Prashu and Nandkeolyar R.I. (2018): A numerical treatment of unsteady three-dimensional hydromagnetic flow of a Casson fluid with Hall and radiation effects.– Results in Physics, vol.11, pp.966-974, https://doi.org/10.1016/j.rinp.2018.10.041.

Received: May 16, 2025
Revised: May 6, 2026